

INFLUENCE OF COMPOSITE LAY-UP ON THE LOAD-CARRYING CAPACITY OF STRUCTURES WITH CLOSED RECTANGULAR CROSS-SECTION

Kuba ROSŁANIEC*, Patryk RÓŻYŁO*

*Faculty of Mechanical Engineering, Department of Machine Design and Mechatronics, Lublin University of Technology,
Nadbystrzycka 36, 20-618 Lublin, Poland

kuba.roslaniec@pollub.edu.pl, p.rozylo@pollub.pl

received 28 November 2024, revised 29 January 2025, accepted 30 January 2025

Abstract: The purpose of this study was to carry out an experimental-numerical research of the influence of the composite layer system on the compressive strength of thin-walled eight-layer composite profiles with closed sections. The subjects of the study were thin-walled composite profiles made of carbon-epoxy composite by autoclave technique. The experimental studies utilized a universal testing machine, an optical deformation measurement system, and a digital microscope with a mobile working head. In parallel with the experimental studies, numerical simulations were conducted using the finite element method. Both the experimental studies and numerical simulations focused primarily on assessing the phenomenon of load-carrying capacity loss. The numerical simulations employed progressive damage analysis, which enabled the analysis of the obtained post-critical equilibrium paths. The research was conducted as part of a project funded by the National Science Centre, project no. 2021/41/B/ST8/00148.

Key words: failure; closed profile; experimental study; FEM; axial compression

1. INTRODUCTION

Thin-walled composite structures are widely used in many industries due to their relatively high strength and stiffness while maintaining low weight and ability to operate in harsh operating conditions [1]. These structures, especially those with closed sections, are mainly designed to carry compressive loads [2,3]. A desirable and common feature of this type of structure is the ability to carry compressive loads even after loss of stability, i.e. after buckling has occurred. In most cases, buckling does not significantly affect the ability to carry the load in the covered state (i.e., the state after buckling has occurred), since the redistribution of stresses in the loaded structure leads to a change in its deformation, which does not significantly reduce the ability to continue working under load conditions. The ability to carry higher loads than those causing buckling significantly increases the operational safety of such structures [4-7]. Some laminates with appropriately selected geometric parameters and ply arrangement are capable of carrying up to several times the buckling load. Increasing the load after buckling can lead to such phenomena as the initiation and propagation of fiber and matrix damage, delamination, and, as a further consequence, increasing the load can lead to a loss of load carrying capacity, that is, the ability of the structure to carry the load due to the development of structural damage [8,9].

The geometry of the cross-section of a composite profile has a direct impact on its strength, stiffness and load response characteristics. There are two basic varieties of composite profiles: closed cross sections [2,3,10] and open cross sections [10-12]. Studies have shown that composites with closed sections have higher strength and significantly higher stiffness compared to profiles with open sections. The higher stiffness is due to higher structural integrity, resulting in better stress distribution and higher resistance to

torsional effects. As a result, these profiles have higher structural stability [13-15].

The layer arrangement and their quantity have a significant impact on the stability and strength of the structure. These properties directly determine the behavior of the loaded structure and its resistance to damage, such as matrix and reinforcement cracking and tearing, as well as resistance to delamination. In most cases, increasing the number of layers enhances the structure's load resistance; however, as the number of layers grows, the total mass of the structure also increases [16-18]. Therefore, an important aspect is the careful selection of the number of layers and their configuration to optimize the strength properties of the profile.

This article focuses on conducting a comparative analysis of the impact of layer arrangement on the phenomenon of failure and the load-carrying capacity of three types of composite columns. These columns, made from carbon-epoxy composite, feature different layer arrangements but have identical cross-sectional geometries. The assessment of the influence of layer configuration on load-carrying capacity was performed using several independent research methods. Experimental tests were conducted using interdisciplinary techniques such as a universal testing machine, an optical deformation measurement system, and acoustic emission monitoring. Computer simulations were carried out using the finite element method in Abaqus® software. The material properties of the analyzed structures were experimentally determined in the following studies [13,19]

The novelty of this work lies in the analysis of the impact of layer arrangement on load-carrying capacity across three configurations with identical closed cross-sections. Experimentally obtained results were compared with those derived from numerical simulations. The primary aim of the study was to compare load-carrying capacities across the three different layer arrangements.

2. RESEARCH OBJECT

The thin-walled composite structures studied were made of carbon-epoxy composite CFRP by autoclave technique, using CY-COM 985-42%-HS-135-305 prepreg tape [20]. This tape is characterized by a width of 305 mm, a volume content of type 985 resin of 42% and a carbon fiber reinforcement with a density of 135 g/m². The tested structures were made by winding the prepreg onto an inner core with winding angles corresponding to the ply configuration. Curing of the composite structure in an autoclave was carried out at a temperature of 177°C and a pressure of 0.6 MPa. A detailed description of the process of manufacturing composite sections with closed sections was presented in the article [21], on the basis of which the present samples were made. Full-load tests were carried out for three different layer configurations in the composite, analyzing the following layer arrangements: 1 – [0/90/0/90]_s; 2 – [45/-45/90/0]_s; 3 – [90/-45/45/0]_s. For each layer configuration in the composite, three actual samples were produced and used in experimental studies, with the following overall dimensions (in mm):

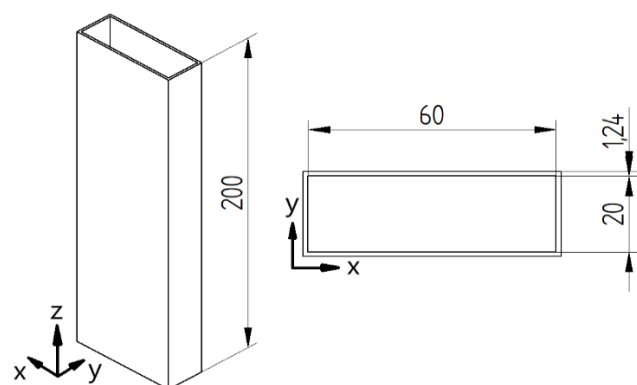


Fig. 1. Overall dimensions of test specimen

Tab. 1. Material properties of the carbon-epoxy composite: average values with standard deviation from a number of material test trials more extensively described in papers [13,19]

Mechanical properties		Strength parameters	
Young's modulus E_1 (MPa)	103014.11 (2145.73)	Tensile strength (0°) F_{tu} (MPa)	1277.41 (56.23)
Young's modulus E_2 (MPa)	7361.45 (307.97)	Compressive strength (0°) F_{cu} (MPa)	572.44 (46.20)
Poisson's ratio ν_{12} [-]	0.37 (0.17)	Tensile strength (90°) F_{tu} (MPa)	31.46 (9.64)
Kirchhoff modulus G_{12} (MPa)	4040.53 (167.35)	Compressive strength (90°) F_{cu} (MPa)	104.04 (7.34)
		Shear strength (45°) F_{su} (MPa)	134.48 (2.71)

In order to develop numerical models that represented the actual structures faithfully, it was necessary to determine the mechanical and strength parameters of the material from which the test specimens were made. This allowed the analysis of the structure's load-carrying capacity and numerical simulations to be carried out in the post-buckling range up to complete failure. The material properties, shown in Table 1, were determined in accordance with current ISO standards using static strength tests. A detailed

description of the procedure for determining material parameters is presented in the article [13]. Numerical models corresponding to the actual structures were developed with a Lamin-type orthotropic model using the determined material properties, using the commercial software Abaqus. This made it possible to compare the results and behavior of the numerical models with experimental results. In the present study, the effect of mechanical couplings, such as torsion and bending of the composite structure, were not considered due to their negligible effect on the operation and behavior of the loaded real structure [22-24].

3. EXPERIMENTAL STUDIES

Experimental studies were carried out at the same time using several interdisciplinary research methods. The basic tool used in the experimental research was a Zwick Z100 universal testing machine [25], which allows recording the behavior of the structure in the covered state until it loses its load-carrying capacity, i.e. the structure's ability to carry the load. Tests carried out with a constant feed rate of the head of the strength machine of 1mm/min at room temperature. Axial compression tests were carried out by placing specimens between special working heads whose flat platforms (crossheads) maintain parallelism throughout the experimental tests. During testing with the testing machine, the Aramis 2D optical deformation measurement system was used. This system allowed non-contact recording of the deformation of the specimen under compression, which eliminates the possibility of interference and measurement inconsistencies arising from contact between the measuring tool and the test piece. The operation of this system is based on the principle of Digital Image Correlation (DIC). The use of this measurement system in the present study made it possible to record phenomena such as buckling but especially failure, which was the focus of the study. Graphical representation of deformations provided a more detailed understanding of the nature of the damage phenomenon. In order to eliminate unwanted image overexposure of the recorded composite columns, filters were used to absorb excess light that could adversely affect the quality of the obtained images. This allowed the elimination of unfavorable optical effects and reflections. In addition, LED reflectors were used to ensure uniform illumination and adequate brightness, which eliminated the problem of uneven illumination [26,27].

Fig. 2. Test stand



Also used in the research was a Keyence VHX-970F digital microscope with a movable head mounted on an articulated arm, which allows observation of defects to identify and evaluate them. This microscope included a VHX-A97FP control console, VHX-

H5M 3D measurement software, VHX-7020 camera, VH-Z20T zoom lens (magnification 20×÷200×), VH-Z00T zoom lens (magnification 0×÷50×) and VHX-S600E tripod. The use of this device made it possible to record high-resolution images on which various forms of damage can be observed, such as warp and fiber discontinuity and material delamination [28,29].

4. NUMERICAL SIMULATIONS

Numerical studies were carried out using the Finite Element Method (FEM). Numerical simulations were performed using the commercial software Abaqus. For each structure analyzed, dedicated numerical models were developed, faithfully reproducing actual structures and experimental tests, based on the „Lamina” type modeling method using the material data shown in Table 1. The material model used in the numerical simulations (Lamina modeling type) enabling an orthotropic approach in composite material modeling. Material properties determined experimentally (shown in Table 1) were implemented under Elastic type properties and Fail Stress type properties. The models represented an eight-layer composite made of carbon-epoxy CFRP material, with layers of equal thickness arranged in three different lay-ups: 1 - [0/90/0/90]s, 2 - [45/-45/90/0]s and 3 - [90/-45/45/0]s. In order to represent the experimental studies, the traverses of the universal testing machine, modeled as non-deformable shell elements, were modeled in the numerical model, which made it possible to incorporate boundary conditions into the numerical model. A numerical model of the composite structure was placed between the non-deformable shell elements. Discrete models of the composite structures were designed using Continuum Shell with SC8R-type finite elements (eight-node general-purpose shell elements with three degrees of freedom (translations) at each node). The traverses of the universal testing machine were modeled using Shell elements of type R3D4 (four-node elements with six degrees of freedom, i.e., three translational and three rotational). The global mesh density of the discrete composite column model was 2 mm, and the composite structure model consisted of 9200 finite elements. For the discrete model of plate elements, the global mesh density was 2.5 mm, and the model consisted of 1120 finite elements.

The FEA-based study used SC8R-type finite elements due to significantly more favorable test results than either S4R or S8R-type shell elements. Due to the high stiffness of the composite profiles, the composite modeling technique using SC8R (Continuum Shell) type elements made it possible to obtain higher convergence in terms of both structural stability and load carrying capacity.

To represent the correct interaction between the composite element and plate elements, contact relations were defined, taking into account contact interaction in the normal and tangential directions. In order to provide the correct interaction between the mating surfaces of the elements, especially in the post-buckling condition, the effect of frictional interaction in the tangential direction was taken into account. A “penalty” contact type was used, with a friction coefficient value of 0.2. Contact in the normal direction was modeled using a so-called “hard” contact of the normal-overclosure type, which allows separation of elements during the course of the numerical analysis.

To reproduce the experimental conditions, boundary conditions were defined at reference points coupled to non-deformable shell elements. For the lower plate, all degrees of freedom of the reference point were locked. On the other hand, for the upper plate, realizing axial compression of the material, the direction on the Z-axis

was left unrestrained, making it possible to introduce displacement of the reference point - thus simulating the phenomenon of axial compression of the composite structure.

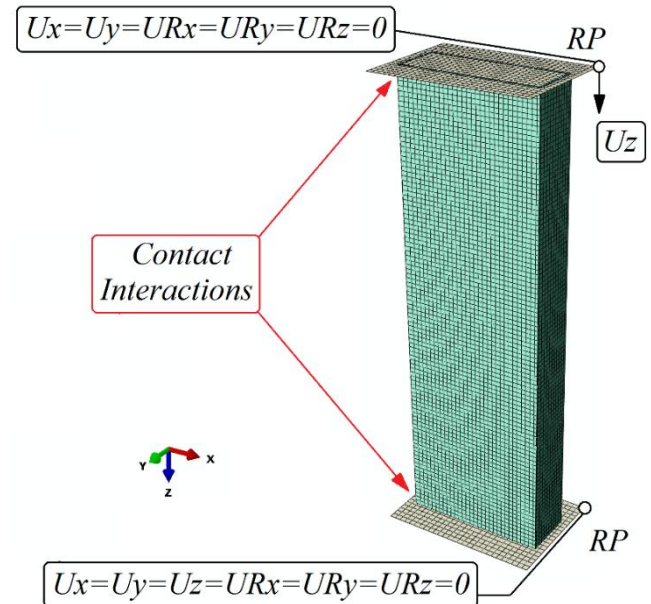


Fig. 3. Numerical model with boundary conditions

Numerical research was carried out in two stages, and in the first stage a model was developed to enable buckling state analysis, in which the force and buckling form of the structure were determined based on the minimum potential energy criterion. The solution of the linear eigenproblem is presented in Eq. (1), and its detailed description is contained in the works [2,8].

$$(K_0^{NM} + \lambda_i K_\Delta^{NM})v_i^M = 0 \quad (1)$$

where: K_0^{NM} - structural stiffness matrix, equivalent to the initial condition, which includes the effects of preloads P^N , K_Δ^{NM} - the differential matrix of initial stress and load stiffness resulting from the incremental loading pattern (Q^N), λ_i - is the eigenvalues, v_i^M - represents the buckling mode, known as the eigenvectors, M and N - the degrees of freedom of the entire model, i - buckling form (mode). The critical load is represented by the equation: $P^N + \lambda_i Q^N$.

The present study didn't focus on the first stage of the research. This stage only served to correctly conduct the target nonlinear structural capacity calculations based on the obtained forms of loss of stability. The target, and the one on which the work focused, stage of numerical research was to conduct nonlinear stability analysis of the structure. In the present analysis, the obtained forms of loss of stability were used and geometric imperfections were taken into account in order to correctly carry out the nonlinear load capacity analysis. This approach makes it possible to reproduce imperfections in the shape of real structures that arise during the manufacturing process. Load simulations in the full load-carrying range were carried out using the Newton-Raphson method, an incremental-iterative method that allows analysis of the structure's behavior in the covered state, taking into account the phenomenon of degradation of the structure's stiffness due to damage initiation and evolution. The method used has enabled the use of an advanced material degradation model known as Progressive Failure Analysis (PFA). Using the Progressive Failure Analysis model [30], taking into consideration the damage initiation criterion based on the

Hashin criterion [31,32], and the damage evolution criterion based on the energy criterion [33,34]. This made it possible to carry out a numerical analysis, taking into account the adverse effects of damage caused by loading the structure on the load carrying capacity of composite structures. The damage initiation condition is achieved when any of the following equations reaches a value of 1:

$$F_f^t = \left(\frac{\hat{\sigma}_{11}}{X^T}\right)^2 + \alpha \left(\frac{\hat{\tau}_{12}}{S^L}\right)^2 = 1, (\hat{\sigma}_{11} \geq 0), \quad (2)$$

$$F_f^c = \left(\frac{\hat{\sigma}_{11}}{X^C}\right), (\hat{\sigma}_{11} < 0), \quad (3)$$

$$F_m^t = \left(\frac{\hat{\sigma}_{22}}{Y^T}\right)^2 + \left(\frac{\hat{\tau}_{12}}{S^L}\right)^2 = 1, (\hat{\sigma}_{22} \geq 0), \quad (4)$$

$$F_m^c = \left(\frac{\hat{\sigma}_{22}}{Y^C}\right)^2 + \left[\left(\frac{Y^C}{2S^T}\right)^2 - 1\right] \frac{\hat{\sigma}_{22}}{Y^C} + \left(\frac{\hat{\tau}_{12}}{S^L}\right)^2 = 1, (\hat{\sigma}_{22} < 0), \quad (5)$$

where: X^T and X^C - tensile and compressive strength in the direction along the fibers, Y^T and Y^C - tensile and compressive strength in the direction perpendicular to the fibers, S^L and S^T - shear strength in the direction along and transverse to the fibers, α - effect of shear stress, $\hat{\sigma}_{11}$, $\hat{\sigma}_{22}$, $\hat{\tau}_{12}$ - the components of the effective stress tensor.

Damage is defined as the loss of effective cross-sectional area [35], so in order to describe the phenomenon of damage, the damage coefficient d was presented in scalar form. A value of this coefficient of 0 indicates that no damage has occurred, while reaching a value of 1 indicates damage to the structure. The effective stress is defined as [36]:

$$\hat{\sigma} = M\sigma = \begin{bmatrix} \frac{1}{1-d_f} & 0 & 0 \\ 0 & \frac{1}{1-d_m} & 0 \\ 0 & 0 & \frac{1}{1-d_s} \end{bmatrix} \begin{pmatrix} \sigma_{11} \\ \sigma_{22} \\ \tau_{12} \end{pmatrix} \quad (6)$$

where: $\hat{\sigma}$ - effective tension, σ - apparent tension (Cauchy nominal), d - damage parameter: fiber, matrix and shear damage, M - damage operator, σ_{ij} - stresses on the appropriate directions.

A model accounting for the degradation of the stiffness matrix coefficients was applied for the analysis of anisotropic materials reinforced with long continuous fibers. Based on equation (6) and the quantitative analysis of the Poisson's ratio degradation [36], the compliance matrix, considering the damage, can be expressed as:

$$F = \begin{bmatrix} \frac{1}{(1-d_f)E_1} & -\frac{\nu_{12}}{E_2} & 0 \\ -\frac{\nu_{12}}{E_1} & \frac{1}{(1-d_m)E_2} & 0 \\ 0 & 0 & \frac{1}{(1-d_s)G_{12}} \end{bmatrix} \quad (7)$$

The damaged stiffness matrix can be expressed as:

$$C = \frac{1}{A} \begin{bmatrix} (1-d_f)E_1 & (1-d_f)(1-d_m)\nu_{12}E_1 & 0 \\ (1-d_f)(1-d_m)\nu_{12}E_2 & (1-d_f)E_2 & 0 \\ 0 & 0 & A(1-d_s)G_{12} \end{bmatrix} \quad (8)$$

The parameter A in the equation is expressed as:

$$A = 1 - \nu_{12}\nu_{21}(1-d_f)(1-d_m) \quad (9)$$

In the case where damage initiation has occurred in the composite material (i.e., when any of the above equations are satisfied), further loading of the composite structure results in damage evolution, leading to the gradual degradation of the composite structure's

stiffness until the loss of load-carrying capacity. Below are the parameters related to the destruction phenomenon, and a detailed description of the damage evolution phenomenon has been presented in the following articles [8,25].

$$d_f = \begin{cases} d_f^t, & \text{if } \hat{\sigma}_{11} \geq 0 \\ d_f^c, & \text{if } \hat{\sigma}_{11} < 0 \end{cases} \quad (10)$$

$$d_m = \begin{cases} d_m^t, & \text{if } \hat{\sigma}_{22} \geq 0 \\ d_m^c, & \text{if } \hat{\sigma}_{22} < 0 \end{cases} \quad (11)$$

$$d_s = 1 - (1 - d_f^t)(1 - d_f^c)(1 - d_m^t)(1 - d_m^c) \quad (12)$$

where: d_f - fiber damage parameter, d_m - matrix damage parameter, d_s - shear damage parameter.

When the damage initiation condition is realized, further loading of the thin-walled composite column will lead to degradation of the material's stiffness parameters. To allow simulation of the evolution of this phenomenon, it is necessary to introduce additional parameters of the damage energy. This process is controlled by damage variables, and its evolution is based on the fracture energy G_c , which is released during damage propagation. In the context of damage evolution, it is required to determine the energy parameters G_c^{ft} , G_c^{fc} , G_c^{mt} and G_c^{mc} , which represent the energies dissipated during damage for the tension and compression of the fiber and matrix. Damage evolution begins when the initiation criterion based on Hashin's criterion is met, which allows progressive failure analysis (PFA) to be performed, as detailed shown in the literature [8,25].

5. RESEARCH RESULTS

The application of experimental and numerical research methods enabled the assessment of the impact of layer configuration on the load-carrying capacity of thin-walled composite structures. Utilizing interdisciplinary research methods allowed for determining the maximum loads that the analyzed structures can withstand. The studies conducted with the use of a universal testing machine facilitated the determination of experimental equilibrium paths, which served as the basis for calculating maximum load capacities (P_f). Three different layer configurations were compared, with three actual structures prepared and tested for each case. The experimentally determined equilibrium paths and those calculated using the finite element method were collated and presented in Figure 4, providing a graphical representation of the differences among the results. The maximum load values obtained through experimental and numerical methods are presented in Table 2. All units of the obtained results have been presented in Newtons (N). The recorded strain results, obtained via the Aramis 2D optical deformation system and expressed as percentages, are presented with an accuracy of three decimal places.

The tests carried out showed that configuration 1 had the highest experimentally determined average limit (failure) load value, achieving about 1.30 times the load of the lowest observed average load-carrying capacity for configuration 3, and nearly 1.17 times the load of the average load-carrying capacity observed for configuration 2 (in experimental tests). Similar trends were observed in the numerical analyses, where the same samples achieved the highest and lowest load-carrying values. The numerical simulations confirmed the results of the experimental studies, indicating that the failure load for configuration 1 was 1.27 times higher than for configuration 3 and approximately 1.17 times higher than for configuration 2.

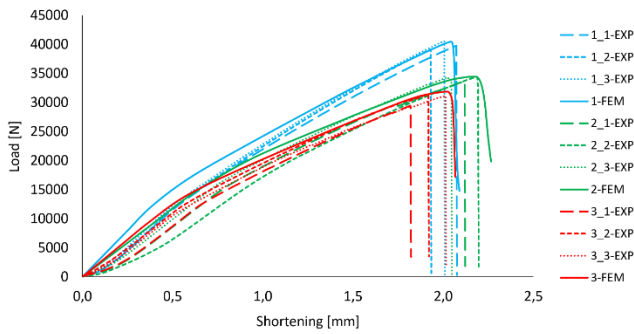


Fig. 4. Summary of post-buckling equilibrium paths

Tab. 1. Failure force values obtained experimentally and numerically

Spec. No Lay-up	1 (N)	2 (N)	3 (N)	EXP Avg.Value (N)	FEM (N)
	[0/90/0/90] _s	39799.60	39150.57		
[45/-45/90/0] _s	33661.53	34416.62	34364.65	34147.60	34456.80
[90/-45/45/0] _s	29448.82	31415.54	31172.51	30678.96	31884.60

The conducted studies demonstrated a high level of agreement between the results obtained from experimental tests and numerical simulations, both qualitatively and quantitatively. The analysis of the equilibrium paths showed a good correlation between the characteristics obtained by experimental and numerical methods. It was observed that the loss of load-carrying capacity occurs at similar failure load values and with comparable shortening in both methods. The similarity in the behavior of the characteristics obtained through the finite element method indicates a high consistency of the numerical model with the experimental results. A quantitative analysis of the load-carrying forces obtained experimentally and numerically showed very good agreement. The failure load values obtained numerically were slightly higher than the average experimental values—about 1.016 times higher for configuration 1, approximately 1.009 times higher for configuration 2, and around 1.039 times higher for configuration 3.

The comparison of the equilibrium path progression revealed that the characteristics obtained through the finite element method display slightly higher force values compared to experimental results, especially noticeable in the early stages of structural loading. This suggests a greater stiffness in the numerical models. Discrepancies between experimental results and numerical simulations are attributed to imperfections in the sample manufacturing methods, which cause minor geometric and structural inaccuracies in the actual composite structures. Nonetheless, these differences are minimal and do not affect the overall quality of the conducted studies.

In the conducted study, it was observed that the analyzed structures failed in areas located near the midpoint of the composite column height. Additionally, it was shown that the thin-walled structures under investigation lose their load-carrying capacity due to layer cracking, matrix rupture, and interlayer delamination, as illustrated in Figure 6. Experimental studies revealed complex failure modes that exhibited varied forms of structural damage. For profiles of types 1 and 3, the predominant damage mechanism was distinct transverse cracking of the layers, perpendicular to the column

height, which results from the specific layer arrangement. This process was further associated with the occurrence of delamination. In contrast, for the second profile type, the primary damage mechanism involved layer cracking at a 45° angle relative to the longitudinal direction of the structure, resulting from the orientation of the laminate's outer layers (45°/-45°), accompanied by delamination phenomena.

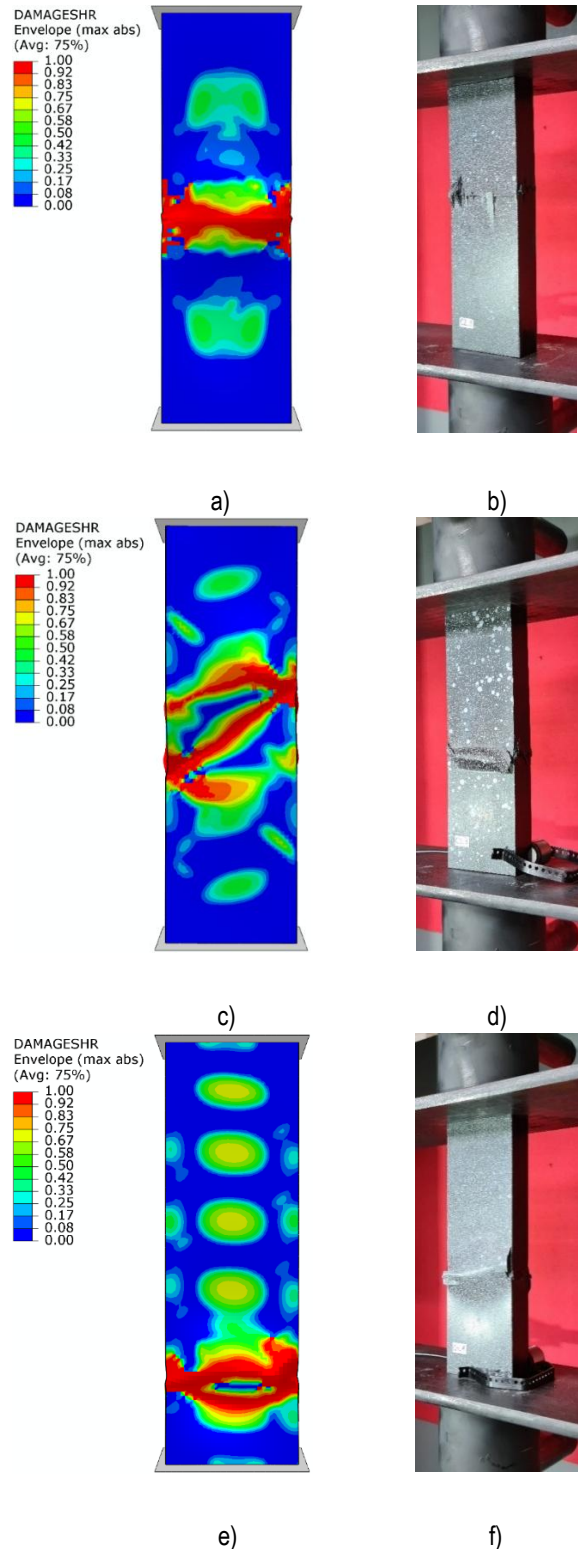


Fig. 5. Comparison of numerical-experimental failure: a) FEM – 1 lay-up, b) EXP – 1 lay-up, c) FEM – 2 lay-up, d) EXP – 2 lay-up, e) FEM – 3 lay-up, f) EXP – 3 lay-up

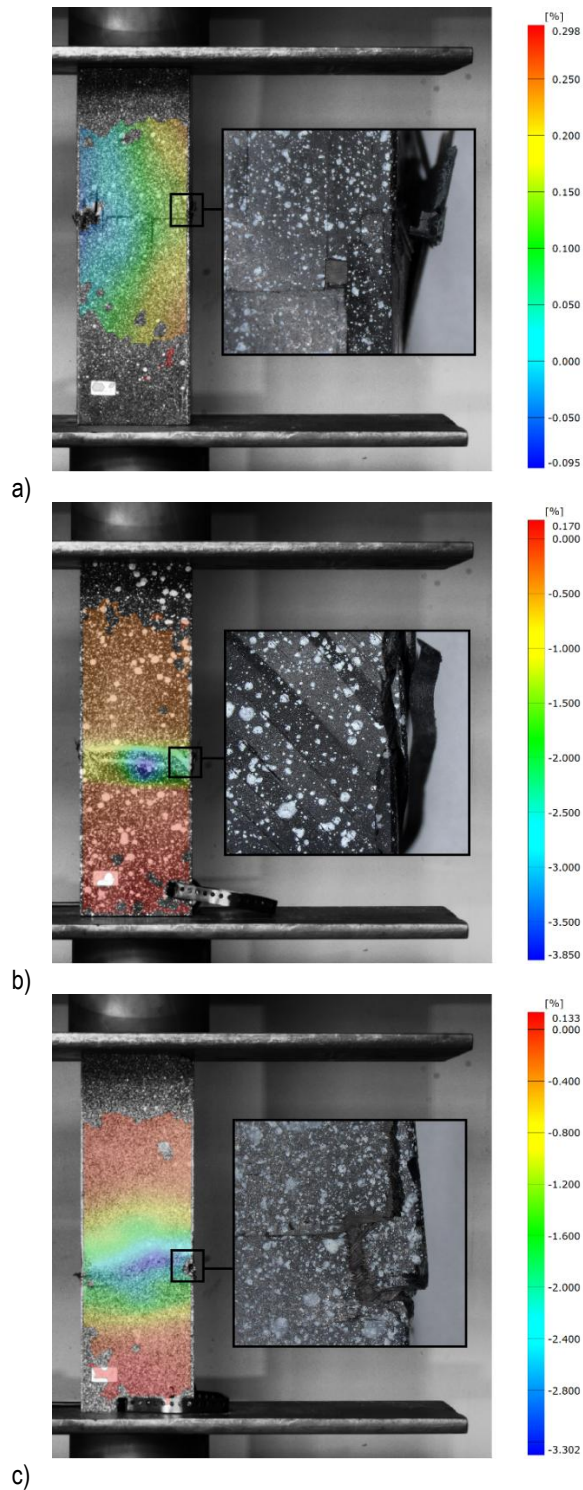


Fig. 6. Damaged structures with graphical visualization of deformations and enlarged representation of selected damage areas: a) 1 lay-up, b) 2 lay-up, c) 3 lay-up

The analysis of the damage forms in the tested profiles, as shown in the figures above, revealed a significant influence of layer arrangement on the nature of the damage. The configuration of layers determines the intensity of damage from cracking as well as the susceptibility to delamination. Despite differences in the types of damage observed, the affected areas remained similar regardless of the layer arrangement in the composite.

The numerical simulations conducted using the finite element method indicated that the outer and inner layers of the laminate are

more susceptible to damage, and consequently, to failure, compared to the central layers of the composite structure. A comparison of the damage levels is illustrated in the figure below, using the type 1 - $[0/90/0/90]_s$ profile as an example:

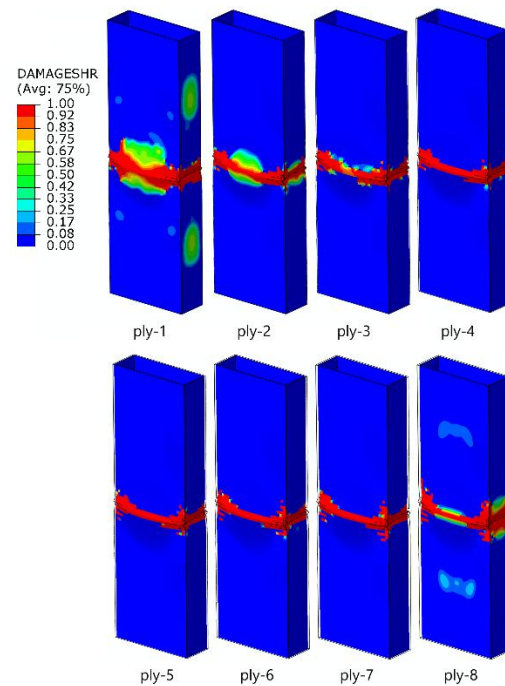


Fig. 7. Comparison of the damage level of individual layers

It was observed that the failure phenomenon is more extensive in the outer layers of the composite, which was confirmed by both numerical simulations and experimental studies. The damage forms obtained provide the basis for the development of more advanced FEM models, such as damage modeling techniques using CZM (Cohesive Zone Model) or XFEM (Extended Finite Element Method), applied to the analysis of delamination and fracture of composite material layers.

6. CONCLUSIONS

The subject of the study was an eight-layer column made of carbon-epoxy composite with a cross-sectional dimension of 60 mm x 20 mm, height of 200 mm, and thickness of 1.24 mm, with three different layer configurations: 1 - $[0/90/0/90]_s$, 2 - $[45/-45/90/0]_s$, 3 - $[90/-45/45/0]_s$. The samples were subjected to axial compression testing using a universal testing machine to determine the load-carrying capacity. The tests were conducted on nine real specimens, with three specimens produced for each layer configuration, and each specimen was tested once until failure.

Numerical simulations using the finite element method were also performed. Proprietary numerical models were developed, using the Lamin model dedicated to composite materials. The developed models reflected the conditions of the experiments carried out and the mechanical properties of the tested profiles, making it possible to analyze their behavior over the full range of loading, up to the complete failure of the structure.

The conducted studies showed that the layer arrangement significantly affects the load-carrying capacity of composite columns. Configuration 1 - $[0/90/0/90]_s$ had the highest load-carrying

capacity, while configuration 3 configuration - $[90/-45/45/0]_s$ had the lowest. Table 2 presents the detailed results of the experimental and numerical studies. The analysis of the obtained results revealed a high level of agreement between the experimentally obtained results and the numerical analysis outcomes. This indicates the high quality and accuracy of the developed numerical models. Additionally, the analysis of equilibrium paths confirms a high level of convergence between the numerical analyses and the conducted tests.

The damage analysis revealed that the most susceptible layers to failure are the outermost and innermost layers of the laminate. The middle layers exhibit less susceptibility to damage, as shown in Figure 7. It was also observed that the primary forms of failure are delamination and layer and matrix cracking, with the damage localized in the area around the midpoint of the composite column's height, as presented in Figure 6.

REFERENCES

- Różyło P, Dębski H. Stability and load-carrying capacity of short composite Z-profiles under eccentric compression. *Thin-Walled Structures*. 2020;157:107019.
- Urbaniak M, Świniarski J, Czapski P, Kubiak T. Experimental investigations of thin-walled GFRP beams subjected to pure bending. *Thin-Walled Structures*. 2016;107(1):397-404.
- Drożdźiel M, Podolak P, Czapski P, Zgórnjak P, Jakubczak P. Failure analysis of GFRP columns subjected to axial compression manufactured under various curing-process conditions. *Composite Structures*. 2021;262:113342.
- Baker A, Dutton S, Donald KD. *Composite materials for aircraft structures*, Reston: American Institute of Aeronautics and Astronautics. 2004.
- Soutis C. Carbon fibre reinforced plastics in aircraft construction, *Materials Science and Engineering*. 2005;412 (1-2):171-176.
- Różyło P, Falkowicz K. Stability and failure analysis of compressed thin-walled composite structures with central cut-out, using three advanced independent damage models. *Composite Structures* 2021;273:114298.
- Banat D, Mania RJ. Failure assessment of thin-walled FML profiles during buckling and postbuckling response. *Composites Part B: Engineering*. 2017;112:278-289.
- Różyło P. Stability and failure of compressed thin-walled composite columns using experimental tests and advanced numerical damage models. *International Journal For Numerical Methods In Engineering*. 2021;122(18):5076-5099.
- Li ZM, Qiao P. Buckling and postbuckling behavior of shear deformable anisotropic laminated beams with initial geometric imperfections subjected to axial compression. *Engineering Structures*. 2015;85:277-292
- Gliszczyński A, Kubiak T. Progressive failure analysis of thin-walled composite columns subjected to uniaxial compression. *Composite Structures*. 2017;169:52-61.
- Dębski H, Samborski S, Różyło P, Wymulski P. Stability and load-carrying capacity of thin-walled FRP composite Z-profiles under eccentric compression. *Materials*. 2020;13(13):2956.
- Różyło P. Failure phenomenon of compressed thin-walled composite columns with top-hat cross-section for three laminate lay-ups. *Composite Structures*. 2023;304(1):116381.
- Różyło P, Smagowski W, Paśnik J. Experimental Research in the Aspect of Determining the Mechanical and Strength Properties of the Composite Material Made of Carbon-Epoxy Composite. *Advances in Science and Technology Research Journal*. 2023;17(2):232-246.
- Różyło P, Rogala M, Paśnik J. Load-Carrying Capacity of Thin-Walled Composite Columns with Rectangular Cross-Section under Axial Compression. *Materials*. 2024;17(7):1615.
- Różyło P, Roslaniec K, Kuciej M. Buckling of Compressed Thin-Walled Composite Structures with Closed Sections. *Advances in Science and Technology Research Journal*. 2023;17(6):63-72.
- Podolak P, Drożdźiel M, Czapski P, Kubiak T, Bienias J. The failure mode variation in post-buckled GFRP columns with different stacking sequences - Experimental damage analysis and numerical prediction. *International Journal of Mechanical Sciences*. 2021;210:106747.
- Calzada KA, Kapoor SG, DeVor RE, Samuel J, Srivastava AK. Modeling and interpretation of fiber orientation-based failure mechanisms in machining of carbon fiber-reinforced polymer composites. *Journal of Manufacturing Processes*. 2012;14(2):141-149.
- Anto AD, Mia S, Hasib MA. The influence of number and orientation of ply on tensile properties of hybrid composites. *Journal of Physics*. 2019;2(2):025002.
- Różyło P. Determined Material Properties within the framework of the National Science Centre project (OPUS) No. 2021/41/B/ST8/00148. <https://doi.org/10.5281/zenodo.7606942>.
- Wymulski P. Numerical and Experimental Study of Crack Propagation in the Tensile Composite Plate with the Open Hole. *Advances in Science and Technology Research Journal*. 2023;17(4):249-261.
- Czapski P, Jakubczak P, Bienias J, Urbaniak M, Kubiak T. Influence of autoclaving process on the stability of thin-walled, composite columns with a square cross-section – Experimental and numerical studies. *Composite Structures*. 2020;250:112594.
- York CB, Almeida SFM. On Extension-Shearing Bending-Twisting coupled laminates. *Composite Structures*. 2017;164:10-22.
- York CB. Coupled quasi-homogeneous orthotropic laminates. *Mechanics of Composite Materials*. 2011;47(4):405-426.
- Rzeczkowski J, Paśnik J, Samborski S. Mode III numerical analysis of composite laminates with elastic couplings in split cantilever beam configuration. *Composite Structures*. 2021;265:113751.
- Różyło P, Dębski H. Failure study of compressed thin-walled composite columns with top-hat cross-section. *Thin-Walled Structures*. 2022;180:109869.
- Dębski H, Różyło P, Wymulski P, Falkowicz K, Ferdynus M. Experimental study on the effect of eccentric compressive load on the stability and load-carrying capacity of thin-walled composite profiles. *Composites Part B*. 2021;226:109346.
- Dębski H, Jonak J. Failure analysis of thin-walled composite channel section columns. *Composite Structures*. 2018;132:567-574.
- Roslaniec K, Różyło P. Stability of Thin-Walled Composite Structures with Closed Sections Under Compression. *Advances in Science and Technology Research Journal*. 2024;18(3):188-199.
- Różyło P. Limit states of thin-walled composite structures with closed sections under axial compression. *Composites Part B: Engineering*. 2024;287:111813.
- Lapczyk I, Hurtado JA. Progressive damage modeling in fiber-reinforced materials. *Composites Part A: Applied Science and Manufacturing*. 2007;38(11):2333-2341.
- Hashin Z, Rotem A. A Fatigue Failure Criterion for Fiber Reinforced Materials. *Journal of Composite Materials*. 1973; 7(4):448-464.
- Hashin Z. Failure Criteria for Unidirectional Fiber Composites. *Journal of Applied Mechanics*. 1980;47(2):329-334.
- Lemaitre J, Plumtree A. Application of Damage Concepts to Predict Creep-Fatigue Failures. *Journal of Engineering Material and Technology*. 1979;101(3):284-292.
- Ribeiro ML, Vandepitte D, Tita V. Damage Model and Progressive Failure Analyses for Filament Wound Composite Laminates. *Applied Composite Materials*. 2013;20:975-992.
- Kachanov L. Time of the Rupture Process under Creep Conditions, *Izv. An SSSR. Otd. Tekh. Nauk*. 1958;8:26-31.
- Laws N, Dvorak GJ, Hejazi M. Stiffness changes in unidirectional composites caused by crack systems. *Mechanics of Materials*. 1983;2(2):127-137.

The research was conducted under project No. 2021/41/B/ST8/00148, financed by the National Science Centre, Poland. This research was funded in whole or in part by National Science Centre, Poland [2021/41/B/ST8/00148]. For the purpose of Open Access, the author has applied a CC-BY public copyright license to any Author Accepted Manuscript (AAM) version arising from this submission.

Kuba Roslaniec:  <https://orcid.org/0000-0002-4093-1702>

Patryk Różyło:  <https://orcid.org/0000-0003-1997-3235>



This work is licensed under the Creative Commons BY-NC-ND 4.0 license.